Oussama Khatib
Artificial Intelligence Laboratory
Stanford University
Stanford, California 94305

Real-Time Obstacle Avoidance for Manipulators and Mobile Robots

Abstract

This paper presents a unique real-time obstacle avoidance approach for manipulators and mobile robots based on the artificial potential field concept. Collision avoidance, traditionally considered a high level planning problem, can be effectively distributed between different levels of control, allowing real-time robot operations in a complex environment. This method has been extended to moving obstacles by using a time-varying artificial potential field. We have applied this obstacle avoidance scheme to robot arm mechanisms and have used a new approach to the general problem of real-time manipulator control. We reformulated the manipulator control problem as direct control of manipulator motion in operational space—the space in which the task is originally described—rather than as control of the task's corresponding joint space motion obtained only after geometric and kinematic transformation. Outside the obstacles' regions of influence, we caused the end effector to move in a straight line with an upper speed limit. The artificial potential field approach has been extended to collision avoidance for all manipulator links. In addition, a joint space artificial potential field is used to satisfy the manipulator internal joint constraints. This method has been implemented in the COSMOS system for a PUMA 560 robot. Real-time collision avoidance demonstrations on moving obstacles have been performed by using visual sensing.

1. Introduction

In previous research, robot collision avoidance has been a component of higher levels of control in hierarchical robot control systems. Collision avoidance has been treated as a planning problem, and research in this area has focused on the development of collision-free path planning algorithms (Lozano-Perez 1980; Moravec 1980; Chatila 1981; Brooks 1983). These algorithms aim at providing the low level control with a path that will enable the robot to accomplish its assigned task free from any risk of collision.

From this perspective, the function of low level control is limited to the execution of elementary operations for which the paths have been precisely specified. The robot's interaction with its environment is then paced by the time cycle of high level control, which is generally several orders of magnitude slower than the response time of a typical robot. This places limits on the robot's real-time capabilities for precise, fast, and highly interactive operations in a cluttered and evolving environment. We will show that it is possible to extend greatly the function of low level control and to carry out more complex operations by coupling environment sensing feedback with the lowest level of control.

Increasing the capability of low level control has been the impetus for the work on real-time obstacle avoidance that we discuss here. Collision avoidance at the low level of control is not intended to replace high level functions or to solve planning problems. The purpose is to make better use of low level control capabilities in performing real-time operations. At this low level of control, the degree or *level of competence* (Brooks 1984) will remain less than that of higher level control.

The *operational space formulation* is the basis for the application of the potential field approach to robot manipulators. This formulation has its roots in the work on end-effector motion control and obstacle avoidance (Khatib and Le Maitre 1978) that has been implemented for an MA23 manipulator at the Laboratoire d'Automatique de Montpellier in 1978. The operational space approach has been formalized by constructing its basic tool, the equations of motion in the operational space of the manipulator end effector.

The International Journal of Robotics Research,
Vol. 5, No. 1, Spring 1986
© 1986 Massachusetts Institute of Technology.

Avidbots Ex1006
Page 1 of 9

Details of this work have been published elsewhere (Khatib 1980; Khatib 1983; Khatib 1985). In this paper, we review the fundamentals of the operational space formulation and the artificial potential field concept. We present the integration of this collision avoidance approach into the operational space control system and its real-time implementation. The extension of this work to link collision avoidance is also developed.

2. Operational Space Formulation

An *operational coordinate system* is a set x of m_0 *independent* parameters describing the manipulator end-effector position and orientation in a frame of reference R_0. For a nonredundant manipulator, these parameters form a set of configuration parameters in a domain of the operational space and constitute a system of generalized coordinates. The kinetic energy of the holonomic articulated mechanism is a quadratic form of the generalized velocities,

$$T(\mathrm{x}, \dot{\mathrm{x}}) = \tfrac{1}{2}\dot{\mathrm{x}}^T \Lambda(\mathrm{x})\dot{\mathrm{x}}, \tag{1}$$

where $\Lambda(\mathrm{x})$ designates the symmetric matrix of the quadratic form, *i.e.*, the kinetic energy matrix. Using the Lagrangian formalism, the end-effector equations of motion are given by

$$\frac{d}{dt}\left(\frac{\partial L}{\partial \dot{\mathrm{x}}}\right) - \frac{\partial L}{\partial \mathrm{x}} = \mathrm{F}, \tag{2}$$

where the Lagrangian $L(\mathrm{x}, \dot{\mathrm{x}})$ is

$$L(\mathrm{x}, \dot{\mathrm{x}}) = T(\mathrm{x}, \dot{\mathrm{x}}) - U(\mathrm{x}), \tag{3}$$

and $U(\mathrm{x})$ represents the potential energy of the gravity. The symbol F is the operational force vector. These equations can be developed (Khatib 1980; Khatib 1983) and written in the form,

$$\Lambda(\mathrm{x})\ddot{\mathrm{x}} + \mu(\mathrm{x}, \dot{\mathrm{x}}) + \mathrm{p}(\mathrm{x}) = \mathrm{F}, \tag{4}$$

where $\mu(\mathrm{x}, \dot{\mathrm{x}})$ represents the centrifugal and Coriolis forces and $\mathrm{p}(\mathrm{x})$ the gravity forces.

The control of manipulators in operational space is based on the selection of F as a command vector. In order to produce this command, specific forces Γ must be applied with joint-based actuators. The relationship between F and the joint forces Γ is given by

$$\Gamma = J^T(\mathrm{q})\,\mathrm{F}, \tag{5}$$

where q is the vector of the n joint coordinates and $J(\mathrm{q})$ the Jacobian matrix.

The decoupling of the end-effector motion in operational space is achieved by using the following structure of control,

$$\mathrm{F} = \Lambda(\mathrm{x})\mathrm{F}^* + \mu(\mathrm{x}, \dot{\mathrm{x}}) + \mathrm{p}(\mathrm{x}), \tag{6}$$

where F^* represents the command vector of the decoupled end effector that becomes equivalent to a *single unit mass.*

The extension of the operational space approach to redundant manipulator systems is discussed in Khatib (1980); Khatib (1983). The integration of active force control for assembly operations is presented in Khatib (1985).

3. The Artificial Potential Field Approach

We present this method in the context of manipulator collision avoidance. Its application to mobile robots is straightforward. The philosophy of the artificial potential field approach can be schematically described as follows:

> *The manipulator moves in a field of forces. The position to be reached is an attractive pole for the end effector and obstacles are repulsive surfaces for the manipulator parts.*

We first consider the collision avoidance problem of a manipulator end effector with a single obstacle O. If x_d designates the goal position, the control of the manipulator end effector with respect to the obstacle O can be achieved by subjecting it to the artificial potential field,

$$U_{art}(\mathrm{x}) = U_{\mathrm{x}_d}(\mathrm{x}) + U_O(\mathrm{x}). \tag{7}$$

This leads to the following expression of the potential

Avidbots Ex1006
Page 2 of 9

energy in the Lagrangian (Eq. 3),

$$U(\mathrm{x}) = U_{art}(\mathrm{x}) + U_g(\mathrm{x}), \tag{8}$$

where $U_g(\mathrm{x})$ represents the gravity potential energy. Using Lagrange's (Eq. 2) and taking into account the end-effector dynamic decoupling (Eq. 6), the command vector F^*_{art} of the decoupled end effector that corresponds to applying the artificial potential field U_{art} (Eq. 7) can be written as

$$\mathrm{F}^*_{art} = \mathrm{F}^*_{\mathrm{x}_d} + \mathrm{F}^*_O, \tag{9}$$

with

$$\begin{aligned} \mathrm{F}^*_{\mathrm{x}_d} &= -\mathrm{grad}[U_{\mathrm{x}_d}(\mathrm{x})], \\ \mathrm{F}^*_O &= -\mathrm{grad}[U_O(\mathrm{x})]. \end{aligned} \tag{10}$$

The symbol $\mathrm{F}^*_{\mathrm{x}_d}$ is an attractive force allowing the point x of the end effector to reach the goal position x_d, and F^*_O represents a *Force Inducing an Artificial Repulsion from the Surface* (FIRAS, from the French) of the obstacle created by the potential field $U_O(\mathrm{x})$. The symbol $\mathrm{F}^*_{\mathrm{x}_d}$ corresponds to the proportional term, *i.e.* $-k_p(\mathrm{x} - \mathrm{x}_d)$, in a conventional PD servo where k_p is the position gain. The attractive potential field $U_{\mathrm{x}_d}(\mathrm{x})$ is simply

$$U_{\mathrm{x}_d}(\mathrm{x}) = \tfrac{1}{2} k_p(\mathrm{x} - \mathrm{x}_d)^2. \tag{11}$$

$U_O(x)$ is selected such that the artificial potential field $U_{art}(x)$ is a positive continuous and differentiable function which attains its zero minimum when $\mathrm{x} = \mathrm{x}_d$. The articulated mechanical system subjected to $U_{art}(\mathrm{x})$ is stable. Asymptotic stabilization of the system is achieved by adding dissipative forces proportional to $\dot{\mathrm{x}}$. Let k_v be the velocity gain; the forces contributing to the end-effector motion and stabilization are of the form,

$$\mathrm{F}^*_m = -k_p(\mathrm{x} - \mathrm{x}_d) - k_v\dot{\mathrm{x}}. \tag{12}$$

This command vector is inadequate to control the manipulator for tasks that involve large end-effector motion toward a goal position without path specification. For such a task, it is better for the end effector to move in a straight line with an upper speed limit.

Rewriting Eq. (12) leads to the following expression, which can be interpreted as specifying a desired velocity vector in a pure velocity servo-control,

$$\dot{\mathrm{x}}_d = \frac{k_p}{k_v}(\mathrm{x}_d - \mathrm{x}). \tag{13}$$

Let V_{max} designate the assigned speed limit. The limitation of the end-effector velocity magnitude can then be obtained (Khatib, Llibre, and Mampey 1978),

$$\mathrm{F}^*_m = -k_v(\dot{\mathrm{x}} - v\dot{\mathrm{x}}_d), \tag{14}$$

where

$$v = \min\left(1, \frac{V_{\max}}{\sqrt{\dot{\mathrm{x}}_d^T \dot{\mathrm{x}}_d}}\right). \tag{15}$$

With this scheme, the velocity vector $\dot{\mathrm{x}}$ is controlled to be pointed toward the goal position while its magnitude is limited to $V_{\max}$. The end effector will then travel at that speed in a straight line, except during the acceleration and deceleration segments or when it is inside the repulsive potential field regions of influence.

4. FIRAS Function

The artificial potential field $U_O(\mathrm{x})$ should be designed to meet the manipulator stability condition and to create at each point on the obstacle's surface a potential barrier which becomes negligible beyond that surface. Specifically, $U_O(\mathrm{x})$ should be a nonnegative continuous and differentiable function whose value tends to infinity as the end effector approaches the obstacle's surface. In order to avoid undesirable perturbing forces beyond the obstacle's vicinity, the influence of this potential field must be limited to a given region surrounding the obstacle.

Using analytic equations $f(\mathrm{x}) = 0$ for obstacle description, the first artificial potential field function used (Khatib and Le Maitre 1978) was based on the values of the function $f(\mathrm{x})$,

$$U_O(\mathrm{x}) = \begin{cases} \frac{1}{2}\eta\left(\frac{1}{f(\mathrm{x})} - \frac{1}{f(\mathrm{x}_0)}\right)^2 & \text{if } f(\mathrm{x}) \leq f(\mathrm{x}_0), \\ 0 & \text{if } f(\mathrm{x}) > f(\mathrm{x}_0). \end{cases} \tag{16}$$

Avidbots Ex1006
Page 3 of 9

The region of influence of this potential field is bounded by the surfaces $f(\mathrm{x}) = 0$ and $f(\mathrm{x}) = f(\mathrm{x}_0)$, where x_0 is a given point in the vicinity of the obstacle and η a constant gain. This potential function can be obtained very simply in real time since it does not require any distance calculations. However, this potential is difficult to use for asymmetric obstacles where the separation between an obstacle's surface and equipotential surfaces can vary widely.

Using the shortest distance to an obstacle O, we have proposed (Khatib 1980) the following artificial potential field;

$$U_O(\mathrm{x}) = \begin{cases} \frac{1}{2}\eta\left(\frac{1}{\rho} - \frac{1}{\rho_0}\right)^2 & \text{if } \rho \leq \rho_0, \\ 0 & \text{if } \rho > \rho_0, \end{cases} \tag{17}$$

where ρ_0 represents the limit distance of the potential field influence and ρ the shortest distance to the obstacle O. The selection of the distance ρ_0 will depend on the end effector operating speed $V_{\max}$ and on its deceleration ability. End-effector acceleration characteristics are discussed in Khatib and Burdick (1985).

Any point of the robot can be subjected to the artificial potential field. The control of a *Point Subjected to the Potential* (PSP) with respect to an obstacle O is achieved using the FIRAS function,

$$\mathrm{F}^*_{(O,psp)} = \begin{cases} \eta\left(\frac{1}{\rho} - \frac{1}{\rho_0}\right)\frac{1}{\rho^2}\frac{\partial\rho}{\partial\mathrm{x}} & \text{if } \rho \leq \rho_0, \\ \mathbf{0} & \text{if } \rho > \rho_0, \end{cases} \tag{18}$$

where $\frac{\partial\rho}{\partial\mathrm{x}}$ denotes the partial derivative vector of the distance from the PSP to the obstacle,

$$\frac{\partial\rho}{\partial\mathrm{x}} = \left[\frac{\partial\rho}{\partial x}\,\frac{\partial\rho}{\partial y}\,\frac{\partial\rho}{\partial z}\right]^T. \tag{19}$$

The joint forces corresponding to $\mathrm{F}^*_{(O,psp)}$ are obtained using the Jacobian matrix associated with this PSP. Observing Eqs. (6) and (9), these forces are given by

$$\Gamma_{(O,psp)} = J^T_{psp}(\mathrm{q})\Lambda(\mathrm{x})\mathrm{F}^*_{(O,psp)}. \tag{20}$$

Fig. 1. An n-ellipsoid with $n = 4$.

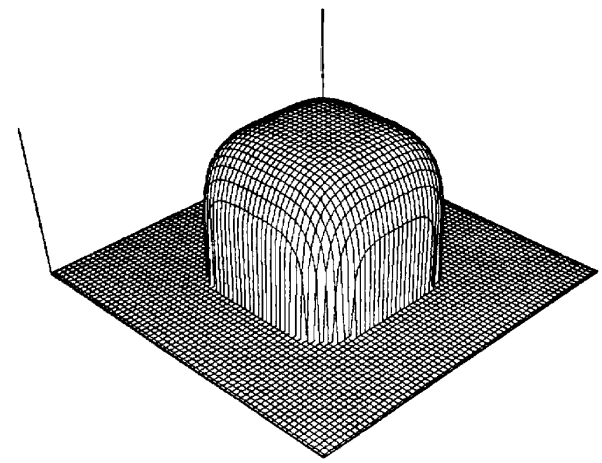

5. Obstacle Geometric Modelling

Obstacles are described by the composition of *primitives.* A typical geometric model base includes primitives such as a point, line, plane, ellipsoid, parallelepiped, cone, and cylinder. The first artificial potential field (Eq. 16) requires analytic equations for the description of obstacles. We have developed analytic equations representing envelopes which best approximate the shapes of primitives such as a *parallelepiped, finite cylinder,* and *cone.*

The surface, termed an *n-ellipsoid,* is represented by the equation,

$$\left(\frac{x}{a}\right)^{2n} + \left(\frac{y}{b}\right)^{2n} + \left(\frac{z}{c}\right)^{2n} = 1, \tag{21}$$

and tends to a parallelepiped of dimensions (2a, 2b, 2c) as n tends to infinity. A good approximation is obtained with $n = 4$, as shown in Fig. 1. A cylinder of elliptical cross section ($2a$, $2b$) and of length $2c$ can be approximated by the so-called *n-cylinder* equation,

$$\left(\frac{x}{a}\right)^{2} + \left(\frac{y}{b}\right)^{2} + \left(\frac{z}{c}\right)^{2n} = 1. \tag{22}$$

The analytic description of primitives is not necessary for the artificial potential field (Eq. 17) since the

Avidbots Ex1006
Page 4 of 9

continuity and differentiability requirement is on the shortest distance to the obstacle. The primitives above, and more generally all convex primitives, comply with this requirement.

Determining the orthogonal distance to an n-ellipsoid or to an n-cylinder requires the solution of a complicated system of equations. A variational procedure for the distance evaluation has been developed that avoids this costly computation. The distance expressions for other primitives are presented in Appendices I through III.

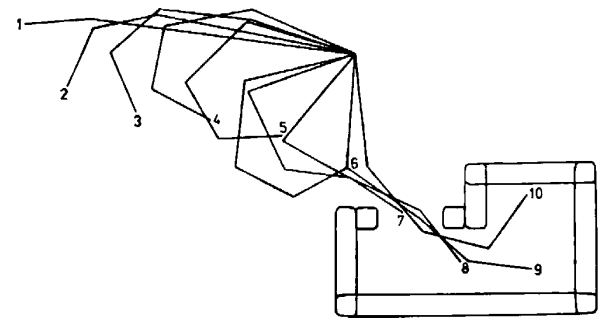

Fig. 2. Displacement of a 4 dof manipulator inside an enclosure.

6. Robot Obstacle Avoidance

An obstacle O_i is described by a set of primitives $\{P_p\}$. The superposition property (additivity) of potential fields enables the control of a given point of the manipulator with respect to this obstacle by using the sum of the relevant gradients,

$$\mathrm{F}^*_{O_i,psp} = \sum_p \mathrm{F}^*_{(P_p,psp)}. \tag{23}$$

Control of this point for several obstacles is obtained using

$$\mathrm{F}^*_{psp} = \sum_i \mathrm{F}^*_{(O_i,psp)}. \tag{24}$$

It is also feasible to have different points on the manipulator controlled with respect to different obstacles. The resulting joint force vector is given by

$$\Gamma_{obstacles} = \sum_j J^T_{psp_j}(\mathrm{q})\Lambda(\mathrm{x})\mathrm{F}^*_{psp_j}. \tag{25}$$

Specifying an adequate number of PSPs enables the protection of all of the manipulator's parts. An example of a dynamic simulation for a redundant 4 *dof* manipulator operating in the plane is shown in the display of Fig. 2.

The artificial potential field approach can be extended to *moving obstacles* since stability of the mechanism persists with a continuously time-varying potential field.

The manipulator obstacle avoidance problem has been formulated in terms of *collision avoidance of links* rather than points. Link collision avoidance is achieved by continuously controlling the link's closest point to the obstacle. At most, n PSPs then have to be considered. Additional links can be artificially introduced or the length of the last link can be extended to account for the manipulator tool or load. In an articulated chain, a link can be represented as the line segment defined by the Cartesian positions of its two neighboring joints. In a frame of reference R, a point $m(x, y, z)$ of the link bounded by $m_1(x_1, y_1, z_1)$ and $m_2(x_2, y_2, z_2)$ is described by the parametric equations,

$$\begin{aligned} x &= x_1 + \lambda(x_2 - x_1), \\ y &= y_1 + \lambda(y_2 - y_1), \\ z &= z_1 + \lambda(z_2 - z_1). \end{aligned} \tag{26}$$

The problem of obtaining the link's shortest distance to a parallelepiped can be reduced to that of finding the link's closest point to a vertex, edge, or face. The analytic expressions of the link's closest point, the distance, and its partial derivatives are given in Appendix I. In Appendices II and III these expressions are given for a cylinder and a cone, respectively.

7. Joint Limit Avoidance

The potential field approach can be used to satisfy the manipulator internal joint constraints. Let $\underline{q}_i$ and $\overline{q}_i$ be respectively the minimal and maximal bounds of the ith joint coordinate q_i. These boundaries can contain q_i by creating barriers of potential at each of the hyperplanes $(q_i = \underline{q}_i)$ and $(q_i = \overline{q}_i)$. The corresponding joint

Avidbots Ex1006
Page 5 of 9

forces are

$$\gamma_{\underline{q}_i} = \begin{cases} \eta\left(\frac{1}{\underline{\rho}_i} - \frac{1}{\underline{\rho}_{i(0)}}\right)\frac{1}{\underline{\rho}_i^2} & \text{if } \underline{\rho}_i \leq \underline{\rho}_{i(0)}, \\ 0 & \text{if } \underline{\rho}_i > \underline{\rho}_{i(0)}, \end{cases} \tag{27}$$

and

$$\gamma_{\bar{q}_i} = \begin{cases} -\eta\left(\frac{1}{\bar{\rho}_i} - \frac{1}{\bar{\rho}_{i(0)}}\right)\frac{1}{\bar{\rho}_i^2} & \text{if } \bar{\rho}_i \leq \bar{\rho}_{i(0)}, \\ 0 & \text{if } \bar{\rho}_i > \bar{\rho}_{i(0)}, \end{cases} \tag{28}$$

where $\underline{\rho}_{i(0)}$ and $\bar{\rho}_{i(0)}$ represent the distance limit of the potential field influence. The distances $\underline{\rho}_i$ and $\bar{\rho}_i$ are defined by

$$\begin{aligned} \underline{\rho}_i &= q_i - \underline{q}_i, \\ \bar{\rho}_i &= \bar{q}_i - q_i. \end{aligned} \tag{29}$$

8. Level of Competence

The potential field concept is indeed an attractive approach to the collision avoidance problem and much research has recently been focused on its applications to robot control (Kuntze and Schill 1982; Hogan 1984; Krogh 1984). However, the complexity of tasks that can be implemented with this approach is limited. In a cluttered environment, local minima can occur in the resultant potential field. This can lead to a stable positioning of the robot before reaching its goal. While local procedures can be designed to exit from such configurations, limitations for complex tasks will remain. This is because the approach has a *local* perspective of the robot environment.

Nevertheless, the resulting potential field does provide the global information necessary and a collision-free path, if attainable, can be found by linking the absolute minima of the potential. Linking these minima requires a computationally expensive exploration of the potential field. This goes beyond the real-time control we are concerned with here but can be considered as an integrated part of higher level control. Work on high level collision-free path planning based on the potential field concept has been investigated in Buckley (1985).

9. Real-Time Implementation

Finally, the global control system integrating the potential field concept with the operational space approach has the following structure:

$$\Gamma = \Gamma_{motion} + \Gamma_{obstacles} + \Gamma_{joint-limit}, \tag{30}$$

where Γ_{motion} can be developed (Khatib 1983) in the form,

$$\begin{aligned} \Gamma_{motion} = J^T(\mathrm{q})\Lambda(\mathrm{q})\mathrm{F}_m^* + \tilde{B}(\mathrm{q})[\dot{\mathrm{q}}\dot{\mathrm{q}}] \\ + \tilde{C}(\mathrm{q})[\dot{\mathrm{q}}^2] + \mathrm{g}(\mathrm{q}), \end{aligned} \tag{31}$$

where $\tilde{B}(\mathrm{q})$ and $\tilde{C}(\mathrm{q})$ are the $n \times n(n-1)/2$ and $n \times n$ matrices of the joint forces under the mapping into joint space of the end-effector Coriolis and centrifugal forces. The symbol $\mathrm{g}(\mathrm{q})$ is the gravity force vector, and the symbolic notations $[\dot{\mathrm{q}}\dot{\mathrm{q}}]$ and $[\dot{\mathrm{q}}^2]$ are for the $n(n-1)/2 \times 1$ and $n \times 1$ column matrices,

$$\begin{aligned} [\dot{\mathrm{q}}\dot{\mathrm{q}}] &= [\dot{q}_1\dot{q}_2\ \dot{q}_1\dot{q}_3\ \ldots\ \dot{q}_{n-1}\ \dot{q}_n]^T, \\ [\dot{\mathrm{q}}^2] &= [\dot{q}_1^2\ \dot{q}_2^2\ \ldots\ \dot{q}_n^2]^T. \end{aligned} \tag{32}$$

In this control structure, dynamic decoupling of the end effector is obtained using the end-effector dynamic parameters (EEDP) $\Lambda(\mathrm{q})$, $\tilde{B}(\mathrm{q})$, $\tilde{C}(\mathrm{q})$ and $\mathrm{g}(\mathrm{q})$, which are configuration dependent. In real time, these parameters can be computed at a lower rate than that of the servo control. In addition, the integration of an operational position and velocity estimator allows a reduction in the rate of end-effector position computation, which involves evaluations of the manipulator geometric model. This leads to a two-level control system architecture (Khatib 1985):

- A low rate *parameter evaluation level* that updates the end-effector dynamic coefficients, the Jacobian matrix, and the geometric model.
- A high rate *servo control level* that computes the command vector using the estimator and the updated dynamic coefficients.

The control system architecture is shown in Fig. 3 where *np* represents the number of PSPs. The Jacobian matrices $J_{psp_j}^T(\mathrm{q})$ have common factors with the end-effector Jacobian matrix $J^T(\mathrm{q})$. Thus, their evaluation does not require significant additional computation.

Avidbots Ex1006
Page 6 of 9

Fig. 3. Control system architecture.

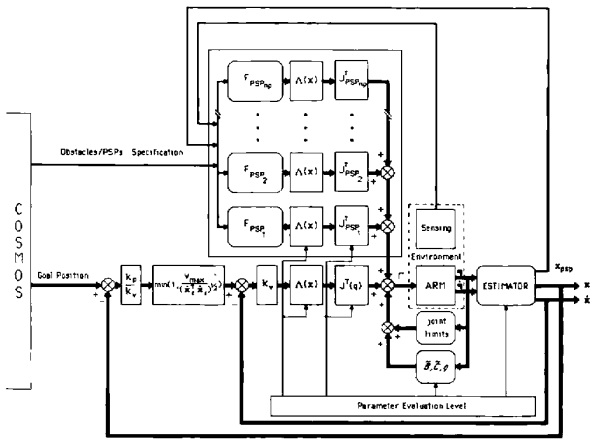

10. Applications

This approach has been implemented in an experimental manipulator programming system *Control in Operational Space of a Manipulator-with-Obstacles System* (COSMOS). Demonstration of real-time collision avoidance with links and moving obstacles (Khatib et al. 1984) have been performed using a PUMA 560 and a Machine Intelligence Corporation vision module.

We have also demonstrated real-time end-effector motion and active force control operations with the COSMOS system using wrist and finger sensing. These include contact, slide, insertion, and compliance operations (Khatib, Burdick, and Armstrong 1985).

In the current multiprocessor implementation (PDP 11/45 and PDP 11/60), the rate of the servo control level is 225 Hz while the coefficient evaluation level runs at 100 Hz.

11. Summary and Discussion

We have described the formulation and implementation of a real-time obstacle avoidance approach based on the artificial potential field concept. Collision avoidance, generally treated as high level planning, has been demonstrated to be an effective component of low level real-time control in this approach. Further, we have briefly presented our operational space formulation of manipulator control that provides the basis for this obstacle avoidance approach, and have described the two-level architecture designed to increase the real-time performance of the control system.

The integration of this low level control approach with a high level planning system seems to be one of the more promising solutions to the obstacle avoidance problem in robot control. With this approach, the problem may be treated in two stages:

- at high level control, generating a global strategy for the manipulator's path in terms of intermediate goals (rather than finding an accurate collision-free path);
- at the low level, producing the appropriate commands to attain each of these goals, taking into account the detailed geometry and motion of manipulator and obstacle, and making use of real-time obstacle sensing (low level vision and proximity sensors).

By extending low level control capabilities and reducing the high level path planning burden, the integration of this collision avoidance approach into a multi-level robot control structure will improve the real-time performance of the overall robot control system. Potential applications of this control approach include moving obstacle avoidance, collision avoidance in grasping operations, and obstacle avoidance problems involving multimanipulators or multifingered hands.

Appendix I: Link Distance to a Parallelepiped

The axes of the frame of reference R are chosen to be the parallelepiped axes of symmetry. The link's length is l and the dot product is $(\cdot)$.

Distance to a Vertex

The closest point m of the line (Eq. 26) to the vertex v is such that

$$\lambda = \frac{(\mathrm{vm}_1) \cdot (\mathrm{m}_1\mathrm{m}_2)}{l^2}. \qquad \text{(A1-1)}$$

Avidbots Ex1006
Page 7 of 9

The link's closest point m is identical to m_1 if $\lambda \leqslant 0$; it is identical to m_2 if $\lambda \geqslant 1$ and it is given by Eq. (26) otherwise. The shortest distance is therefore,

$$\rho = \begin{cases} [\rho_1^2 - \lambda^2 l^2]^{1/2}, & \text{if } 0 \leqslant \lambda \leqslant 1, \\ \rho_1, & \text{if } \lambda < 0, \\ \rho_2 & \text{if } \lambda > 1, \end{cases} \tag{A1-2}$$

where ρ_1 and ρ_2 are the distance to the vertex from m_1 and m_2, respectively. The distance partial derivatives are

$$\frac{\partial \rho}{\partial \mathrm{x}} = \left[\frac{x}{\rho}\,\frac{y}{\rho}\,\frac{z}{\rho}\right]^T. \tag{A1-3}$$

Distance to an Edge

By a projection in the plane perpendicular to the considered edge (xoy, yoz, or zox), this problem can be reduced to that of finding the distance to a vertex in the plane. This leads to expressions similar to those of (A1-1)–(A1-3) with a zero partial derivative of the distance *w.r.t.* the axis parallel to the edge.

Distance to a Face

In this case, the distance can be directly obtained by comparing the absolute values of the coordinates of m_1 and m_2 along the axis perpendicular to the face. The partial derivative vector is identical to the unit normal vector of this face.

Appendix II: Link Distance to a Cylinder

The frame of reference R is chosen such that its z-axis is the cylinder axis of symmetry and its origin is the cylinder center of mass. The cylinder radius and height are designated by r and h, respectively.

Distance to the Circular Surface

The closest point of the link (Eq. 27) to the circular surface of the cylinder can be deduced from the distance to a vertex considered in the xoy plane and by allowing for the radius r.

Distance to the Circular Edges

The closest distance to the cylinder circular edge can be obtained from that of the circular surface by taking into account the relative z-coordinate of m to the circular edge, *i.e.*, $(z + h/2)$ for the base and $(z - h/2)$ for the top. The distance partial derivative vector results from the torus equation,

$$[x^2 + y^2 + (z \pm h/2)^2 - r^2 - \rho^2]^2 = 4r^2[\rho^2 - (z \pm h/2)^2]. \tag{A2-1}$$

This vector is

$$\frac{\partial \rho}{\partial \mathrm{x}} = \left[\zeta\frac{x}{\rho}\,\zeta\frac{y}{\rho}\,\frac{z \pm h/2}{\rho}\right]^T, \tag{A2-2}$$

with

$$\zeta = \frac{x^2 + y^2 + (z \pm h/2)^2 - r^2 - \rho^2}{x^2 + y^2 + (z \pm h/2)^2 + r^2 - \rho^2}. \tag{A2-3}$$

The distance to the planar surfaces is straightforward and can be simply obtained as in Appendix I.

Appendix III: Link Distance to a Cone

In this case, the frame of reference R is chosen such that its z-axis is the cone axis of symmetry and its origin is the center of the cone circular base. The cone base radius, height and half angle are represented respectively by r, h, and β.

Distance to the Cone-Shaped Surface

The problem of locating $m(x, y, z)$ is identical to that for the cylinder case. The distance can be written as

$$\rho = z \sin(\beta) + (\sqrt{x^2 + y^2} - r)\cos(\beta). \tag{A3-1}$$

Avidbots Ex1006
Page 8 of 9

The partial derivatives come from the equation,

$$x^2 + y^2 = r_z^2, \tag{A3-2}$$

where

$$r_z = \tan(\beta)[h + \rho \sin(\beta) - z]. \tag{A3-3}$$

They are

$$\frac{\partial \rho}{\partial \mathrm{x}} = \left[\frac{x}{r_z \tan(\beta)} \; \frac{y}{r_z \tan(\beta)} \; \frac{1}{\sin(\beta)}\right]^T. \tag{A3-4}$$

The problem of the distance to the cone circular edge is identical to that of the cylinder circular edge in Appendix II. The distance to the cone vertex is solved as in Appendix I.

Acknowledgments

Tom Binford and Bernie Roth have encouraged and given support for the continuation of this research at Stanford University. I thank also Harlyn Baker, Peter Blicher, and Jeff Kerr for their help in the preparation of the original manuscript.

References

Brooks, R. 1983. Solving the find-path problem by good representation of free space. *IEEE Sys., Man Cyber.* SMC-13:190–197.

Brooks, R. 1984 Aug. 20–23, Kyoto, Japan. Aspects of mobile robot visual map making. *2nd Int. Symp. Robotics Res.*

Buckley, C. 1985. *The application of continuum methods to path planning.* Ph.D. Thesis (in progress). Stanford University, Department of Mechanical Engineering.

Chatila, R. 1981. *Système de navigation pour un robot mobile autonome: modélisation et processus décisionnels.* Thèse de Docteur-Ingénieur. Université Paul Sabatier. Toulouse, France.

Hogan, N. 1984 June 6–8, San Diego, California. Impedance control: an approach to manipulation. 1984 *Amer. Control Conf.*

Khatib, O., Llibre, M. and Mampey, R. 1978. Fonction decision-commande d'un robot manipulateur. *Rapport No. 2/7156.* DERA/CERT. Toulouse, France.

Khatib, O. and Le Maitre, J. F. 1978 September 12–15, Udine, Italy. Dynamic control of manipulators operating in a complex environment. *Proc. 3rd CISM-IFToMM Symp. Theory Practice Robots Manipulators,* 267-282. Elsevier. 1979.

Khatib, O. 1980. *Commande dynamique dans l'espace opérationnel des robots manipulateurs en présence d'obstacles.* These de Docteur-Ingénieur. École Nationale Supérieure de l'Aéronautique et de l'Espace (ENSAE). Toulouse, France.

Khatib, O. 1983 December 15–20, New Delhi. Dynamic control of manipulators in operational space. *6th CISM-IFToMM Congress Theory Machines Mechanisms,* 1128–1131.

Khatib, O., et al. 1984 June, *Robotics in three acts* (Film). Stanford University. Artificial Intelligence Laboratory.

Khatib, O. 1985 September 11–13, Tokyo. The operational space formulation in robot manipulators control. *15th Int. Symp. Indust. Robots.*

Khatib, O. and Burdick, J. 1985 November, Miami, Florida. Dynamic optimization in manipulator design: the operational space formulation. *ASME Winter Annual Meeting.*

Khatib, O., Burdick, J., and Armstrong, B. 1985. *Robotics in three acts–Part II* (Film). Stanford University, Artificial Intelligence Laboratory.

Krogh, B. 1984 August, Bethlehem, Pennsylvania. A generalized potential field approach to obstacle avoidance control. *SME Conf. Proc. Robotics Research: The Next Five Years and Beyond.*

Kuntze, H. B., and Schill, W. 1982 June 9–11, Paris. Methods for collision avoidance in computer controlled industrial robots. *12th ISIR.*

Lozano-Perez, T. 1980. Spatial planning: a configuration space approach. *AI Memo 605.* Cambridge, Mass. MIT Artificial Intelligence Laboratory.

Moravec, H. P. 1980. *Obstacle avoidance and navigation in the real world by a seeing robot rover.* Ph.D. Thesis. Stanford University, Artificial Intelligence Laboratory.

Avidbots Ex1006
Page 9 of 9